Crashworthiness behavior assessment and multi-objective optimization of horsetail-inspired sandwich tubes based on artificial neural network

Moslem Rezaei Faraz, Shahram Hosseini, Amirreza Tarafdar, Mojtaba Forghani, Hamed Ahmadi, Neil Fellows & Gholamhossein Liaghat

Published online: 05 Oct 2023.

Submit your article to this journal

Article views: 1122

View related articles

View Crossmark data

Citing articles: 11 View citing articles

Taylor & Francis
Taylor & Francis Group

ORIGINAL ARTICLE

OPEN ACCESS

Check for updates

Crashworthiness behavior assessment and multi-objective optimization of horsetail-inspired sandwich tubes based on artificial neural network

Moslem Rezaei Faraz[a], Shahram Hosseini[a] , Amirreza Tarafdar[b], Mojtaba Forghani[c], Hamed Ahmadi[a], Neil Fellows[d], and Gholamhossein Liaghat[d]

[a]Department of Mechanical Engineering, Tarbiat Modares University, Tehran, Iran; [b]Department of Mechanical Engineering, Syracuse University, New York, USA; [c]Department of Mechanical Engineering, Stanford University, Stanford, California, USA; [d]School of Engineering, Computing, and Mathematics, Faculty of Technology, Design, and Environment, Oxford Brookes University, Oxford, UK

ABSTRACT

The crashworthiness behavior of horsetail-inspired sandwich tubes was analyzed in this study. Multilayer perceptron (MLP) algorithms with the Levenberg-Marquardt training algorithm (LMA) were used to predict force-displacement curve and optimize the geometrical parameters according to minimum peak crushing force and specific energy absorption. Based on the non-dominated sorting genetic algorithm II (NSGA-II) optimization results, the specimen with four core tubes and a thickness of 1 mm, and a height of 92 mm has the optimal crashworthiness performance. Finally, the optimal specimen is fabricated and the results of the numerical and MLP methods are validated versus experimental approach.

1. Introduction

Due to their specific strength and SEA capabilities, thin-walled structures are being used more and more in the automotive to reduce the fatal and serious injuries of vulnerable road users (VRU), transportation, and aerospace industries [1–5]. The results of previous analytical [2, 6, 7], experimental [8–10], and computational studies [3, 11, 12] have demonstrated that Energy absorption and crashworthiness depend on many structural and materials parameters, including, metal type, fabric/matrix type, fabrication technology, structural geometry, dimension and loading conditions [13–15]. Due to their excellent mechanical characteristics, aluminum has been investigated by many authors over the previous years [16, 17]. Today, aluminum is still used to fabricate energy absorbers, despite the availability and application of composite and polymer materials for use in energy absorption applications. Based on their ductility features, aluminum tubes under axial loadings disperses kinetic energy through a variety of plastic deformation mechanisms by generating concertina and diamond deformation patterns [18]. Additionally, in recent decades, the effects of tube geometry (i.e. round, triangle, square, and rectangular) on the thin-walled energy-absorbing response have been extensively investigated.

Ruyang Yao et al. [19] provides a comprehensive review on thin-walled multi-cell structures and materials (TWMCSM) for energy absorption. By overviewing a lot of related researches, TWMCSM are found to provide outstanding energy absorption performance compared with their conventional counterparts. At the end of this research, the authors concluded, combining both of the active and passive safety strategies to design adaptive TWMCSM should be a meaningful direction in the future researches.

According to the study by Nia and Hamedani [20], on the evaluation of energy absorption of singular tubes with various cross-sections, tubes with circular cross-sections perform the best. On the other hand, Palombini [21] reported that sections with complex and special shapes showed more crushing and energy absorption properties than conventional single tubes did. Researchers have been looking to optimize the design of aluminum crushing tubes to minimize the drawbacks of aluminum tubes, such as their high pick crushing force (PCF) and unstable deformation, (i.e. global buckling) [22]. Theoretical, computational, and experimental approaches have been developed to improve the efficiency of the designs [23–28]. The multi-cell thin-walled aluminum tube can improve crashworthiness parameters such as PCF, mean crushing force (MCF), total energy absorption (EA), and specific energy absorption (SEA) benefiting from the interactions among their components [29]. As a result, several multi-cell structures have been studied recently. For instance, Vinayagar and Kumar [30] investigated the performance of bi-tubular structures under quasi-static axial loading, including an external circular tube and an internal tube with various cross-sections. The findings of this study demonstrated that the hexagonal inner tube configuration has a more impressive capacity to absorb energy due to the higher number of corners. In another investigation by Liu

et al. [29], the impact response of a full aluminum sandwich structure with a star core was examined. The interaction between the structure's components was shown to significantly boost the crashworthiness characteristics of the sandwich structure. In addition, it was revealed that optimizing the geometry of the structure by Non-Dominated Sorting Genetic Algorithm- II (NSGA-II) based on maximizing the SEA and minimizing the PCF as the most important parameters in energy absorbing structures. According to the results, the value of SAE increased by 8% and the value of PCF decreased by 12%.

In addition to multi-cell sandwich structures, other geometries, such as auxetic structures and foams have been used to improve the crashworthiness behavior of energy absorber structures [31, 32]. Oloumi et al. [33] by examining the hybrid structure of auxetic steel tubes with foam as the core and composite layers which was wrapped around the steel tubes, showed the failure mechanisms and crashworthiness were enhanced and the value of SEA is increased by the hybridization of GFRC with auxetic cellular steel tubes than conventional ones.

Although the energy absorption performance of sandwich structures has significantly enhanced, it appears that optimizing the geometrical characteristics of energy absorbing sandwich structures results into strengthening crashworthiness characteristics, considerably. Such as many fields of researches, looking at nature can attribute to further improvement of energy absorption capacity of thin-walled sandwich structures [34]. Inspiration from biological organisms is a promising way which benefits researchers from designing and optimizing the geometry of energy absorbing structures like horsetail [35], bamboo [36], spongy bone, and human vessel [3] (shown in Figure 1), have undergone years of evolution and have been tailored to be able to adapt to a variety of extreme environments. For instance, Xiao Y et al. [35] evaluated numerically the multicellular structure obtained from the horsetail structure under axial loading using the LS-DYNA finite element code. The outcomes
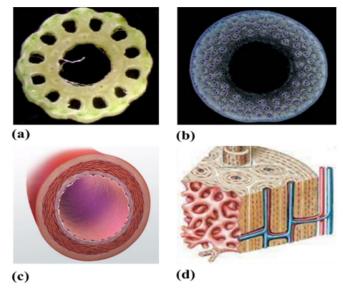
demonstrate that the number of cells, internal wall diameter, and wall thickness of horsetail-bionic thin-walled structures (HBTS) have a significant impact on the failure rate of HBTS. Based on the obtained results, the HBTS with 16-cells, which was the most number of cells, has the best efficiency in absorbing the energy among the six different types of specimens investigated.

Recently, among the bio-inspired multicellular structures, sandwich tube structures have been investigated intensively, due to their ease of manufacturing and promising performance. Liang et al. [25] characterized the crushing behavior of a hierarchical sandwich structure inspired from the outer layer of bones under a quasi-static compression loading. The proposed hierarchical configuration was a hybrid CFRP/aluminum hollow tube. The results progressive folding which leads to a stable crushing behavior, increasing the SEA and EA. Also, the hybrid tube packing net CFRP tubes owns better crashworthiness characteristics. But for this structure with the materials used, it is not possible to say clearly what the results will be by changing the geometrical parameters. Therefore, Optimization is very necessary. In our previous studies [9, 22], the energy absorbing capabilities of bio-inspired hybrid sandwich structure (Al/CFRP, Al/PP) were evaluated. Based on the parametric studies results, specimens containing aluminum components showed progressive crushing behavior, high SEA and crushing force efficiency (CFE), under the axial quasi-static and low velocity impact loading. Due to the existence of several of geometrical variables, finding the optimal design numerically or experimentally by a trial and error process would be costly due to time and manufacturing costs [25].

To address this challenge, machine learning (ML) and artificial neural networks (ANN) algorithms such as multilayer preceptor (MLP) are promising ways to optimize the geometry of the bio-inspired sandwich tubes [37–44]. Moreover, it is noteworthy that MA and ANN approaches are widely used in classification and regression problems and handle numerical and categorical responses well [45–48]. An ANN is composed of numerous nodes (or neurons) connected with one another [45, 49, 50]. The activation function, which is represented by each node, is a particular output function. The network's output is affected by the network structure, network connection modes, weight, and activation function. The functioning of biological neural networks served as inspiration for the design of neural networks [51–53]. ANN is excellent at processing noisy data sets and has great accuracy. As a result, ANN has been widely used in various fields, including material, automation, and condition monitoring. Zhixiang Li et al. [51] using machine learning techniques, predicted and optimized the energy absorption performance of the corrugation-reinforced multi-cell square tube (CMST). Two numerical criteria, i.e. SEA and PCF, and a categorical criterion, i.e. deformation mode, were used to assess the energy absorption performance of the CMST under different geometric parameters. According to this study the geometric parameters have a linear and non-linear effect on the PCF and SEA, respectively. Also, by removing unstable deformation modes based on the prediction of machine learning algorithms the optimum geometry has obtained.

In order to design a high-efficiency energy absorber, predicting an accurate force-displacement curve is the key

Figure 1. Illustration of biological structures inspiriting bio-mimetic energy absorbers a) horsetail, b) bamboo, c) human vessel, and d) spongy bone [3].

factor to optimize the crashworthiness parameters corresponding to bio-inspired energy absorbing sandwich structures [54]. Based on previous investigation, the SEA and PCF are critical parameters to optimize [29, 51]. Moreover, considering different biological structures of the horsetail plant (see Figure 1), it can be seen that the different types of horsetail plant have different internal structures in terms of thickness, and the number of cells between internal and external shells.

In this paper, with a new perspective on horsetail structure (see Figure 2a), the crashworthiness response of the full aluminum sandwich tube under quasi-static axial loading is investigated. According to Figure 2a, the number of core tubes, the thickness of components is considered as a variable geometrical parameter. Moreover, due to the direct effect of the height on the axial compression behavior, the height is selected as a variable as well as the number of core tubes. MLP algorithm with Levenberg-Marquardt's training algorithm is adopted as a new approach to predict the force-displacement curve and optimize the structural characteristics of the bio-inspired sandwich tube. A multi-objective optimization method is applied with respect to the maximal SEA and minimal PCF on the second hierarchical sandwich tube. For this purpose, firstly, to ensure the accuracy of the simulation process, three single hollow tubes, including the core, inner, and outer tubes, and a bio-inspired sandwich tube were simulated, and the obtained results were compared with the corresponding experimental results. Then, a pre-defined number of sandwich tubes have

been simulated using LS-DYNA (a commercial non-linear FE program) to generate the data for inputting into the MLP algorithm. The data is extracted from the force-displacement curves obtained from the simulation. In order to demonstrate the effects of the geometrical parameters the Levenberg-Marquardt's training algorithm (LMA) from the neural network fitting app of MATLAB (a matrix based mathematical solution software) is utilized to train the algorithms. The SEA and PCF values are the predicted outputs of the neural network based on the inputs of tube thickness, height, and number of core tubes. The optimum structural characteristics are obtained by employing the Non-Dominated Sorting Genetic Algorithm-II (NSGA-II) corresponding to the specimen which has higher SEA and lower PCF. Subsequently, the force-displacement curve is predicted by Levenberg-Marquardt's algorithm corresponding to the optimized specimen. Based on the optimized geometrical features, the sandwich tube is prepared experimentally to characterize the quasi-static compression behavior. Finally, the force-displacement curves are derived through experimental and numerical approaches related to the optimized specimen. Then, the derived force-displacement curves are compared to validate the results and demonstrate the optimum geometrical characterizations.

2. Design approach

The goal of the design optimization of horsetail-inspired sandwich tube with hierarchical core attributes to enhance
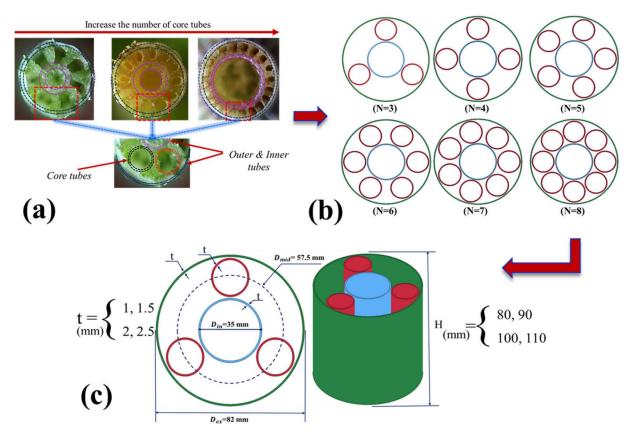

Figure 2. a) Horsetail plant structure with different number of internal cells and different wall thickness [3], b) Schematic of sandwich tubes with different number of core tubes and, c) variable geometrical parameters.

the energy absorption performance while maximizing the SEA and minimizing the PCF [29]. The reason to adopt the SEA as a goal parameter comes from the fact that the optimal design of the energy absorbers should have the highest possible energy absorption with the lowest weight, which leads to lowering the cost and consuming the energy and material. The PCF is known as a critical factor which has impacts on the safety of passengers. In other words, by reducing the peak crushing force, energy absorption structures can ensure compliance with these regulations and standards, thereby enhancing the marketability and acceptance of the product. Additionally, mimicking biological structures is a promising way to enhance the structural performance, such as the internal structure of a horsetail plant. From Figure 2a, it can be observed that the number of inner cells and wall thicknesses of horsetail plant internal components vary. These differences in various horsetail plant species lead to the investigation of the effects of various wall thickness and number of core tubes on crashworthiness behavior of bio-inspired sandwich tubes. Besides, the height of the sandwich tubes influences the crushing response under the axial compression loading. Therefore, it can be claimed that these parameters have the potential to be considered as geometrical variables to improve crashworthiness behavior of horsetail-inspired sandwich tubes. As mentioned before, circular cross-section is considered for sandwich tube components, due to the better performance than other cross-sections such as square, rectangular, hexagonal and so on.

In this research, 96 samples with different geometrical parameters are simulated using the LS-DYNA finite element code. The models incorporated 4 different tube heights ($H = 80$, 90, 100, 110 mm). Then, for samples with the same height, the number of the core tubes was modified from 3 to 8 tubes, in increments of 1 ($N = 3$, 4, 5, 6, 7, 8). Then, for each specimen with the specified height and number of core tubes, the thickness of the components are varied from 1, 1.5, 2 and 2.5 mm for each specimen. Therefore, the total number of numerical models are 96 ($4*6*4 = 96$). The geometry of the different models is shown in Figure 2b and c.

Using the MLP with Levenberg-Marquardt's training algorithm, the PCF and SEA values are predicted for different types of specimens with $80 \leq H \leq 110$ mm and $1 \leq t \leq 2.5$ mm and $3 \leq N \leq 8$. Then, the optimized specimen is designed using the multi-objective genetic algorithm based on highest SEA and lowest PCF. Finally, the force-displacement curve is predicted by LMA algorithm corresponding to the optimized specimen. The detail of the design approach is shown in Figure 3.

3. Machine learning techniques and model selection

3.1. Artificial neural network

An artificial intelligence-based technique known as an artificial neural network (ANN) can be used to recognize complicated phenomena and provide solutions to issues that are intractable by current techniques.
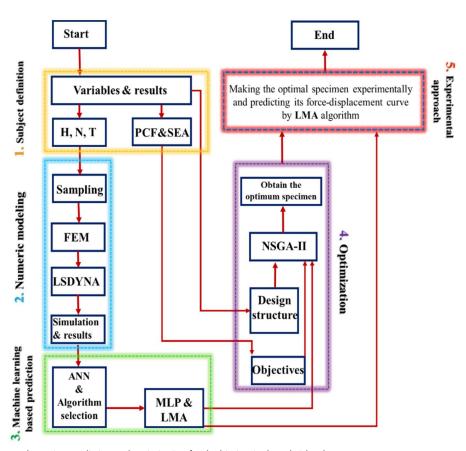

Figure 3. Flow chart of energy absorption prediction and optimization for the bio-inspired sandwich tube.

In this research, the MLP is used to estimate PCF and the SEA values for different compressed sandwich tube structures and force-displacement curve of optimization specimen. The input data, for the MLP algorithms, is the number of core tubes, the tube height, and the tube wall thickness. The PCF and the SEA values obtained from the numerical models are used to training the MLP. Three neuron layers are used in the MLP, with the first layer defined as the input layer, the second layer as the hidden layer, and the third layer as the output layer (see Figure 4). The Levenberg-Marquardt algorithm was utilized in the learning process. The Levenberg-Marquardt method, also known as damped least squares (DLS), is known for its quick calculation and minimum memory utilization [43]. One of the most critical parameters in ANN is determining the number of neurons or, in other words, layer size. This parameter has
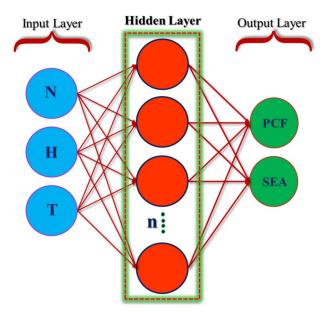
a significant effect on the accuracy of the results. In addition to its high speed the Levenberg-Marquardt algorithm has good accuracy in calculating the results using different numbers of neurons. In the results and discussions section, the effect of layer size on the accuracy of the results is discussed in detail.

3.2. Genetic algorithm (GA)

Choosing the optimal structure is one of the main goals of this research. A non-dominated sorting genetic algorithm II (NSGA-II) has been used to select the optimal dimensions. The genetic algorithm is one of the most potent optimization algorithms that can be used to optimize several parameters when there is one or more objective functions [29]. In the research [55] NSGA-II and MOP-SO algorithms for optimization of a system operation with two functions are compared. According to the presented results, it can be concluded that according to the stop conditions, which is the same for the two algorithms, the NSGA-II is performed better than the MOPSO algorithm. Also, in a part of research [56] that is done about water network, the results of optimization show that the NSGAII algorithm were slightly better than the results of MODE and the results of the MOPSO were weaker than others. Therefore, in this research NSGA-II is considered to optimize the defined functions. Here the objective function is to minimize the PCF and maximize the SEA simultaneously. In order to use the genetic algorithm, separate data cannot be used; because this algorithm selects random values in the defined interval. Therefore, the functions taught in MLP are used as the objective function in the genetic algorithm. A schematic of the used algorithm is shown in Figure 5.

4. Finite element simulation

The non-linear finite element simulation code LS-DYNA (utilizing double-precision) was selected to simulate the loading of the specimens and extract the force displacement curves. The extracted data was input into the machine learning

Figure 4. A schematic diagram of a Multilayer Perceptron (MLP) neural network with n neurons.
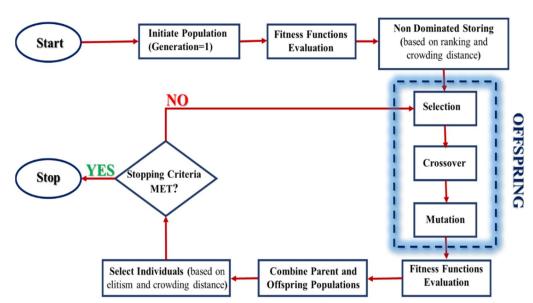
Figure 5. Flow chart of Genetic Algorithm with all steps involved.

algorithms to optimize the geometry parameters and specify the optimum specimen based on genetic algorithms.

4.1. Geometry and boundary conditions

As shown in Figure 6, the Al tubes were simulated as shell elements with 4-node under Belytschko-Tsay formulation utilizing five integration points across the tubes thickness. The tubes were drawn based on the midline position of the tubes (mean value of the tube diameter) with thicknesses set of 1, 1.5, 2, and 2.5 mm around the midline position. A mesh study was performed on the loading of individual tubes, with convergence obtained for all tube sizes when utilizing a mesh size of 1 mm. The final models incorporated the tubes in the pre-configured arrangements, Figure 6, with loading applied between upper and lower rigid plates. The lower plate was fully fixed with the upper plate given a BOUNDARY_PRESCRIBED_MOTION-RIGID in the longitudinal direction of the tubes with a rate of 5 mm/min. These settings reflected the experimental load conditions.

4.2. Material model

The modified_piecewice_linear_plasticity (MAT 123) model in LS-DYNA is good for modeling aluminum alloys [22]. This model enables elastic-plastic behavior to be defined using stress strain curves at different strain rates. Based on previous studies, strain rate in the range of $[10^{-4}\text{-}10^3]$ $(\frac{1}{s})$ has not effect on plastic deformation in Al tubes [9]. It is worth mentioning that two approaches can be mentioned as methods of defining the failure strain in aluminum components: 1- using the RTCL yield criterion to define the effective failure strain. 2- Defining yield stress and using a stress-strain curve.

4.3. Contact definition

Two contact algorithms were defined in the numerical models to prevent the tubes going through themselves, CONTACT AUTOMATIC SINGLE SURFACE was applied to the tubular elements. To prevent the tubes going through each other or through the plates a CONTACT_AUTOMATIC_SURFACE_TO_SURFACE was chosen to them. The static and dynamic coefficients between all surfaces was considered to 0.4 and 0.35, respectively.

5. Experimental procedure

5.1. Material characterization

The purpose of this study is to examine the effects of an aluminum-based circular hybrid multi-cell on the crashworthiness characteristics of tubular sandwich energy absorbers. To this aim, it used tubes made of extruded aluminum alloy 6061-T6. The physic-mechanical properties of aluminum alloy are summarized in Table 1.

5.2. Test procedure

Quasi-static compression test was employed to examine the specimen's crashworthiness behavior to consider variability in the force–displacement data, the compression tests were repeated three times. Crashworthiness characteristics including PCF and SEA were extracted from the force–displacement curves.

For this purpose, a Universal Test Machine (UTM) for quasi-static testing is performed with a load cell capacity of 300 kN (shown in Figure 7). The specimens were positioned between the upper and lower platens (plates) and loaded at a rate of 5 mm/min. Care was taken to ensure the center axes of the samples were aligned with the center position of the upper and bottom platens.

Table 1. Mechanical properties of aluminum tubes [22].

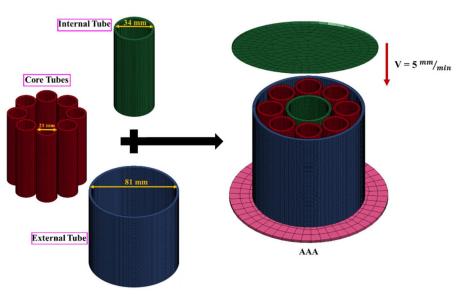| Property	Young's moduli (GPa)	yield stress (MPa)	Density (kg/m3)	Poisson's ratio
Value	70	260	2700	0.33

Figure 6. Simulation of the full aluminum multi-cell sandwich tube.

6. Result and discussion

6.1. Simulation of sandwich tubes

LS-DYNA software was used to simulate the crushing of various sandwich tube configurations to generate the force-displacement curves. From the curves, the maximum SEA and the minimum PCF were obtained and used as outputs in the ANN. As mentioned in Section 2, 96 models have been made to study the effects of the number of core tubes ($N = 3, 4, 5, 6, 7, 8$), the tube thickness ($t\_1 = 1$, $t\_2 = 1.5$, $t\_3 = 2$, $t\_4 = 2.5$ mm), and the tube height ($H = 80, 90, 100, 110$ mm).

According to previous research [9, 22], the kinetic energy that is applied to the bio-inspired aluminum sandwich tubes,
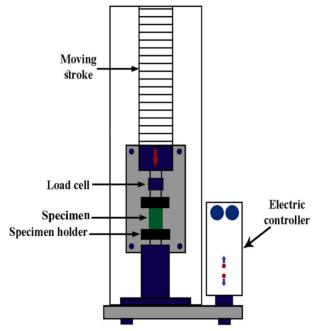
is absorbed through various crushing mechanisms, including progressive folding, plastic deformation, local buckling, and the formation of plastic hinges. Moreover, the kinetic energy interactions between the components are absorbed through friction and interaction forces between the core, inner, and outer tubes.

As a preliminary study, it is necessary to evaluate the accuracy of the simulation process of this research by comparing the numerical versus experimental results. For this reason, the crushing behavior of a horsetail-inspired sandwich and three single hollow tubes (the core, inner, and outer tubes) are validated separately under quasi-static loading, separately. The height and thickness of all tubes are considered 90 mm and 1.2 mm, respectively. It should be noted that each test is repeated three times.

To simulate the sandwich tube, firstly, single hollow tubes were simulated. Then, based on the validated models of single hollow tubes, the components are integrated to generate the horsetail-inspired sandwich tube model.

As shown in Figure 8, the number of folds, shape of n-gons (from the top view), and deformation mechanisms related to single tubes and sandwich tubes have been correctly predicted. Additionally, the load-displacement curves resulting from the numerical study are greatly matched with the trend of the experimental curve (see Figure 9). From Figure 9, it can be seen that the finite element models predict the PCF and the SEA values very accurately, with an error lower than 5%.

After validating the numerical simulation, the 96 defined specimens were simulated. For instance, Figure 10 illustrates the failure behavior of the six bio-inspired sandwich tubes with different numbers of core tubes. By observing the crushed samples, it can be seen that number of core tubes has an important role in controlled the absorption of energy. With an increase of the number of cores, the interaction generated among the components of the sandwich tube
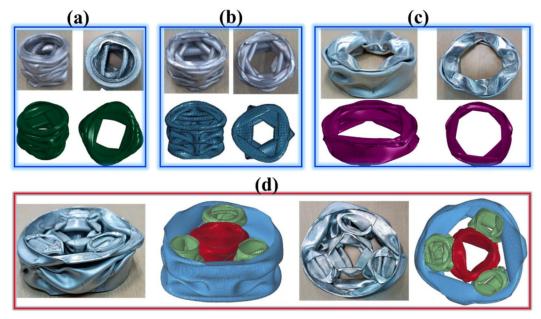

Figure 7. Schematic of the quasi-static test setup (UTM) [22].

Figure 8. Status of Quasi-static compression of experiments and simulation of single hollow tubes a) Core, b) Inner, c) Outer, and d) Sandwich tube.
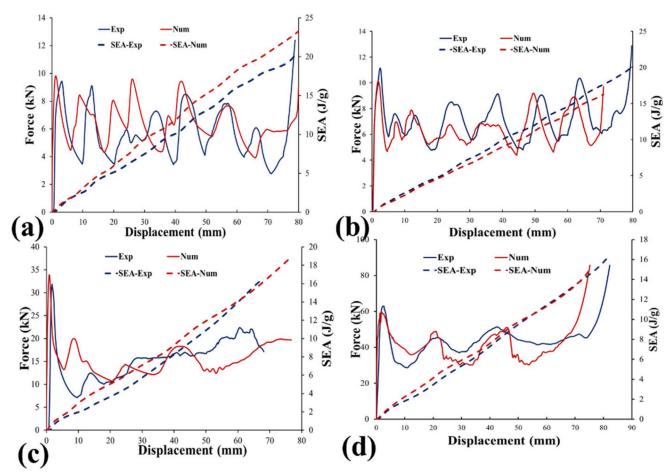
Figure 9. Force-displacement and SEA-displacement curves of single hollow tubes a) Core, b) Inner, c) Outer, and d) Sandwich tube.
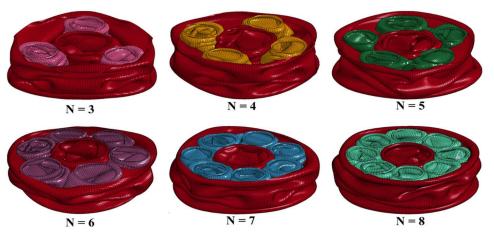

Figure 10. Comparison of axial crushing modes of bio-inspired sandwich tubes with different number of core tubes.

has increased. This phenomenon causes the specific progressive folding of inner and outer tubes. This folding pattern can demonstrate the energy absorbing behavior of sandwich tube.

The force-displacement curves obtained from the models are compared in Figure 11. Generally, it can be seen that changing the thickness of the tubes has a greater effect on the energy absorbing behavior than changing the height of the specimens. The loading capacity and elastic stiffness of the structures improve as the thickness of the sandwich tube components increases. According to Figure 11, the

force-displacement curves related to the specimens with lower thickness drop sharply after the force touches PCF. However, the energy absorption behavior in specimens with a 2.5 mm thickness differs from specimens with other thicknesses. It can be seen after the force reaches to the initial peak, the load drops and then increase up to the PCF.

This phenomenon causes a significant different in the PCF values, which the PCF for the specimens with 2.5 mm thickness is much higher than those with lower thickness. Additionally, comparing the results for the specimens with
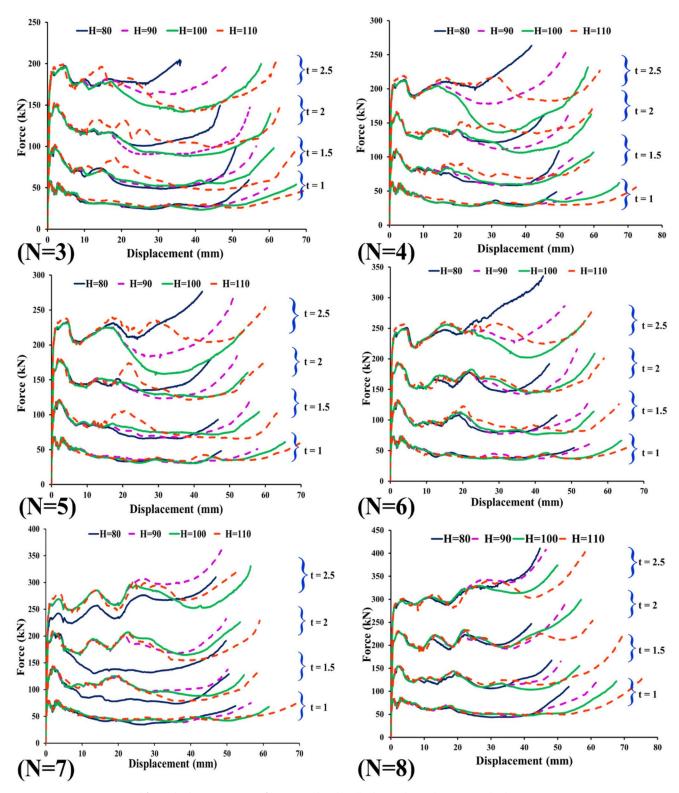
Figure 11. Comparative numerical force–displacement curves of bio-inspired multi-cell tubes under axial quasi-static loading.

same number of cores but different thickness shows that increasing the thickness leads to decrement of crush length. This circumstances is due to the limited space among the components within the sandwich tube. So, increasing the thickness causes a decrease of space between components. Thus, the force-displacement curve rises more quickly due to quicker interaction between the tubes. Considering the force-displacement diagrams, it can be observed that this

phenomenon plays a more prominent role in samples with a shorter height and a larger number of core tubes. On the other hand, it is obvious that increasing the height of the sandwich tubes leads to increment of crush length.

When comparing the results corresponding to the specimens with identical height and thickness, it can be seen that increasing the number of cores leads to an increased load capacity and therefore maximum PCF recorded.

To clarify the effects of geometrical parameters, the amount of PCF and SEA are presented in Figure 12. As mentioned before, for the components with the same number of core tubes, the effect of thickness is very significant.

For these samples, it can be seen that with increasing thickness, the peak crushing force and specific energy absorption increases almost linearly. Also, we can see that for components with the same number of cores and equal thickness, the effect of height is small. But this is not the case in the specific energy absorption parameter, because the length of the samples has a direct effect on the crash length, which causes a change on the SEA value.

6.2. Machine learning and MLP algorithm

In this study MLP algorithm was utilized to predict the PCF and SEA of the sandwich structures and force-displacement curve of optimization specimen under axial quasi-static loading. It should be noted that two separate MLP networks with the different numbers of input and output data were used, one for predicting the PCF and SEA and the other for predicting the force-displacement curve. The chosen machine learning algorithm is capable of handling both regression and classification problems [45]. In this case, as described in section 3.1, the Multilayer Perceptron (MLP) Neural Network with Levenberg-Marquardt training algorithm utilizing one hidden layer was adopted from the neural network fitting tool in the MATLAB software. The number of neurons utilized in a neural network is one of the most important parameters in its design. The size of the layer has a significant effect on the accuracy of the neural network's responses (including the prediction of the PCF and SEA values and the force-displacement curve).

In this case the hidden layer was set to have a different number of nodes ranging from 1 to 15. Generally, to measure the accuracy of the results obtained from the neural network parameters like the Regression (R-value) is used. The R-value measures the correlation between the outputs and targets. Figure 13 depicts a graph of R-values in relation to

layer size for training, validation, and target values. An R-value of 1 means a close relationship and 0 value means a random relationship.

As can be observed, 14 neurons ($n = 14$) or higher shows a better response compared to lower values.

Note that, although the R-value is used for multiple linear regression, coefficient of determination (R^2) is a better term than R-value to Easier to understand [57]. For single and multiple linear regressions, R^2 is used. The evaluation parameter is defined as:

$$R^2 = 1 - \frac{\sum_{i=1}^{N}(y_i - \bar{y}_i)^2}{\sum_{i=1}^{N}(y_i - \bar{y})^2} \qquad \text{Eq.1}$$

Where N is the number of specimens, y_i and $\bar{y}_i$ are true and predicted values for the ith specimen, respectively, $\bar{y}$ is the mean of the true values of N specimens [51]. The higher the value of the R^2 parameter, the higher the accuracy of the predicted model. The ideal value of this parameter is equal to 1.

The SEA and PCF values, which are derived from the force-displacement curve, are considered as multiple regressions problems. So, the coefficient of determination (R^2) is introduced to evaluate the performance of the prediction of the SEA and the PCF.

In this research, the R^2 of the MLP models is evaluated both in the training and test data. As two output data, the R^2 value for the SEA and PCF values are shown in Figure 14. For the PCF and SEA prediction, this model have high R^2 in the training and test set, which is higher than 0.99. In fact, the accuracy acquired from the training set is frequently incredibly high, hence the findings from the test set should receive greater attention. As can be seen, the value of R^2 for the test data is greater than the training data. In addition, a total of 70% of the datasets are utilized for training, 15% for validation, and 15% for testing.

Finally, after ensuring the accuracy of the results, a function is required to predict the two parameters SAE and PCF
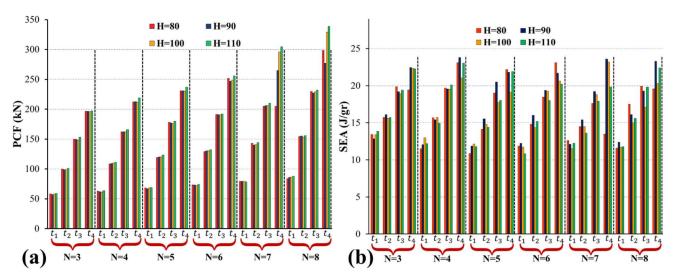

Figure 12. Comparison of a) PCF and b) of sandwich tubes under axial quasi-static loading.
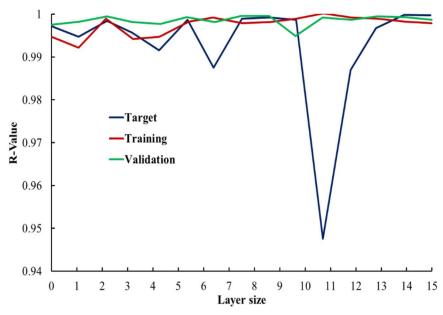
Figure 13. R-value according to layer size in the MLP neural network.
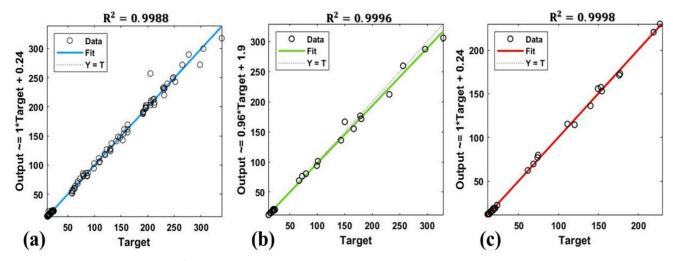

Figure 14. PCF and SEA regression diagram for a) Training data, b) Validation data, and c) Test data.

for different values of T, H, and N, which is discussed in the following.

Figures 15 and 16 display the values of the PCF and the SEA generated by the Multilayer Perceptron (MLP) Neural Network corresponding to the different tube thicknesses ($1 \leq t \leq 2.5$), tube heights ($80 \leq H \leq 110$), and number of core tubes ($3 \leq N \leq 8$), respectively. These results were obtained by using the Levenberg-Marquardt algorithm, which was discussed in Section 3.1.

Based on the SEA and PCF diagrams with constant thickness, changing the height of the specimens do not have much effect on SEA and PCF. But it is great to mention that changing the height for some specimens with $t > 2$ mm has an almost linear effect on PCF values (samples with $N = 6, 7, 8$). It also has had non-linear effect on this parameter for samples with $N = 3$, 4. On the other hand, for samples with $t < 2$ mm, the value of this parameter is almost constant according to the height.

Also, by examining the SEA curves, it can be concluded that the trend of changes of this parameter according to the height for specimens with $N = 3$, 4, 5, and with the same thickness ($t > 2$ mm) is almost the same, so that the value of this parameter increases with the height of the specimens. At first, it was accompanied by an increase, then it decreased, and finally it increased. However, in samples with a thickness of $t < 2$ mm, the value of this parameter first increases and then decreases as the height increases. Also, It can be seen the SEA changes are almost the same for samples with $N = 6$, 7, $t < 2$ mm and samples with $N = 7$, 8 and $t > 2$ mm. in other words, the values of SEA has direct relation with the height of the samples with $N = 6$, 7 and $t < 2$ mm, so that the SEA first increases then decreases. On the other hand, the specimens with $N = 7$, 8 and $t > 2$, the SEA increases in the initial stage and in the following it decreases, and finally it increases. This behavior was
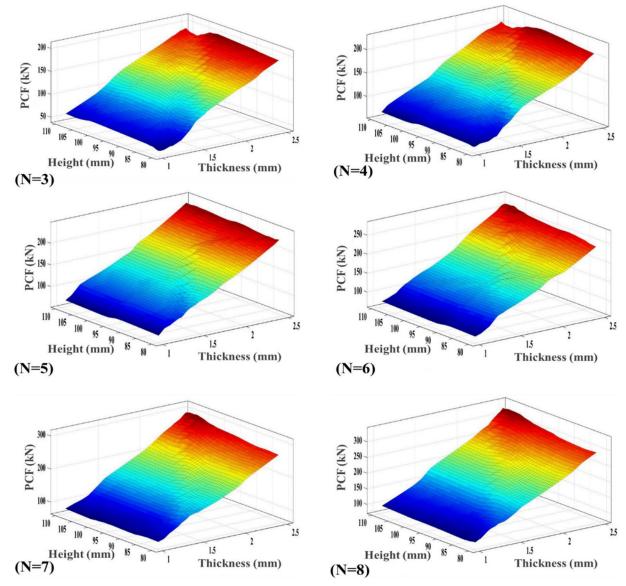
Figure 15. PCF value predicted by MLP neural network for samples with different H, T, and N values.

observed in the simulation results corresponding to the 96 simulated specimens.

In the following, it will be discussed how to use a genetic algorithm to investigate the optimal specimen among all generated specimens.

6.3. Multi objective optimization

As an objective function, it is vital to maximize the SEA of the structure, corresponding to the crashworthiness optimization problem. However, it is also crucial that the PCF of the structure stays within a predetermined acceptable range. Therefore, another objective function that is highly desired is to minimize the PCF. The optimization problem can be expressed using the following multi-objective optimization formulations while taking into account these two distinct design requirements, see Equation 2.

The non-dominated sorting genetic algorithm II is used to conduct the multi-objective optimization design of a

hierarchical sandwich tube after acquiring the values of PCF and SEA for the specimens defined by the ANN algorithm (NSGA-II). In this research, the optimization objectives are defined in a way where the PCF value is minimized and the SEA value is maximized. The problem is described as following:

$$
\begin{cases}
\min\left(PCF, \ -SEA\right) \\
X_L \leq X \leq X_U
\begin{cases}
X = T, \ N, \ H \\
X_L = \ \min(T, \ N, \ H) \\
X_U = \max(T, \ N, \ H)
\end{cases}
\end{cases}
\quad \text{Eq.2.}
$$

How closely a particular solution adheres to the ideal solution to the desired problem is determined by the fitness function, which is also known as the evaluation function. It can be shown that increasing the generation results in reducing the difference between the best fitness and mean fitness values (see Figure 17). Based on the results extracted from the genetic algorithm, the bio-inspired sandwich tube
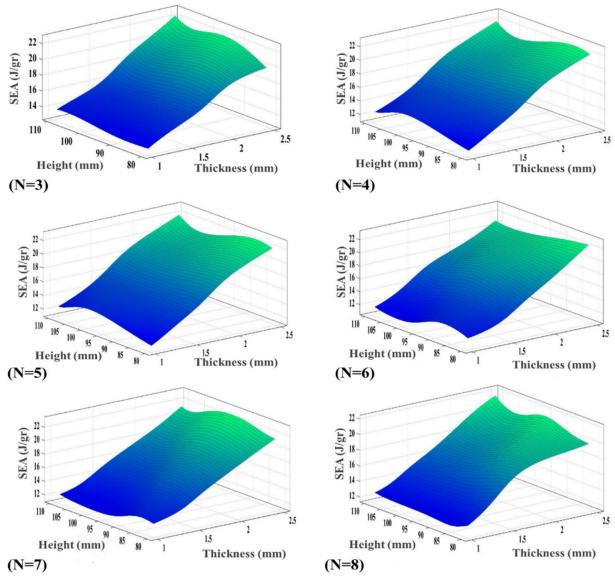
Figure 16. SEA value predicted by MLP neural network for samples with different H, T, and N values.

with four core tubes, a height of 92 mm, and a thickness of 1 mm is the optimal specimen among all the samples.

6.4. Experimental specimen and development of a MLP-based force-displacement prediction model

To validate the accuracy of the optimization process, a quasi-static compression test was conducted to compare the crashworthiness behavior of the optimized sandwich structure with the numerical simulation. It is worth mentioning that the experimental specimen has tested three times. To simulate of crashworthiness behavior of the experimental sandwich tube specimen, firstly, all single hollow tubes, including outer, inner, and cores tubes, are simulated. Then, as mentioned in section 4.3 by using the appropriate static friction coefficient, the simulation of horsetail-inspired sandwich tube is completed. The crushing history and folding mechanism of the optimized sandwich tube is shown in Figure 18. From Figure 18-a1, the initial local buckling is

observed in the upper part of the external tube. Due to the interaction effects between the external and core tubes, the sandwich tube continues to fold from the location where the initial local buckling is observed. In the following (Figure 18-a3) the progressive folding occurs from the upper part of the initial folding pattern, due to the initiation of the progressive folding of the inner and core tubes. Because of increased density of material in upper part of the sandwich tube (creating a resistance to buckling), the folding pattern is progressed through lower parts of the sandwich tube. Due to the interaction between the components of the sandwich tube and increment of material density inside the specimen, the external tube experiences three folds with four corners ($N=4$) where the sides of each fold has equal length (i.e. square shape). While, the folding pattern shape is triangular corresponding to the inner tubes

Considering the results shown in Figure 18 and comparing the obtained results in earlier research [9, 22], it can be concluded that the interaction between components had very good effects on the folding process of the outer tube and
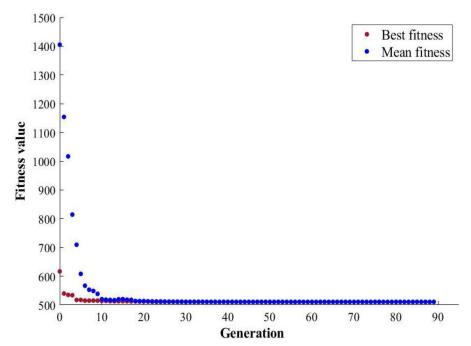
Figure 17. The best fitness value vs. the number of generations in the GA.
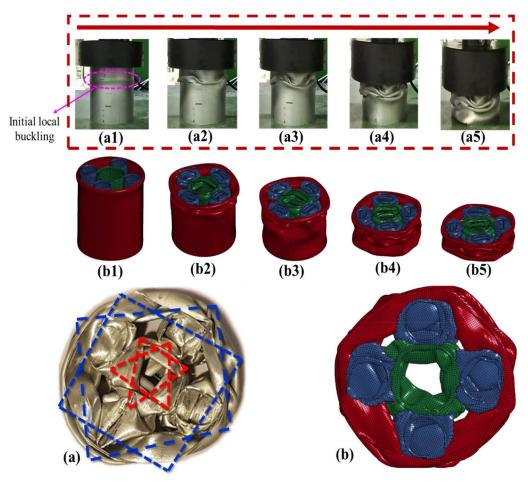
Figure 18. Comparison of axial crushing modes of optimized sandwich tube from the a) experimental, and b) numerical results.

increasing the sides of its N side. On the other hand, this structure causes the deterioration of the fold of the inner tube compared to folding pattern of single hollow tube.

By comparing the FEM and experimental results, it can be seen that the FE model predicts the progressive folding pattern well. Figure 18-b1, presents the initial local
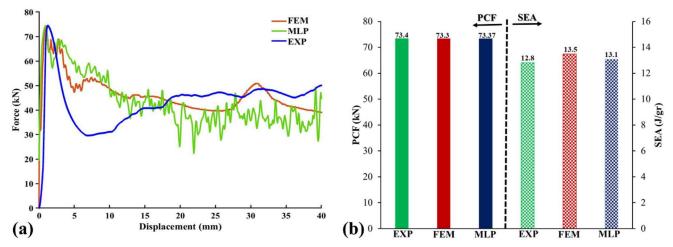
Figure 19. a) Force-displacement curves and b) PCF and SEA value of the optimized specimen based on experimental, numerical, and MLP results.

buckling of the external tube. From the crushing snapshots (Figure 18-b2 to b5), it can be seen that the FE model is showing very similar results to that obtained experimentally in terms of folding and buckling.

As mentioned before, the ability to predict acceptable outputs in accordance with data training is one of the specific applications of neural networks. In order to predict the force-displacement curves corresponding to the optimized specimen, first, a MLP network with $n = 14$ (the number of neurons in the hidden layer) was made, like to the network that predicted the PCF and the SEA. Second, all internal points of force-displacement curves related to the 96 specimens (each curve has 537 points) in the FE analysis were defined as input data's in the MLP creating 51552 datasets. The force-displacement curves information used in the MLP was set to 40 mm total displacement (The lowest displacement value among 96 numerical force-displacement curves). Figure 19a shows the results of the MLP derived force displacement curve in comparison to the experimental and numerical results for the optimized sandwich configuration. As can be seen, the peak loads in all three methods have close values. Additionally, the force-displacement curves follow the same general trend for all three results. However, the experimental result is a little different compared to the numerical and MLP results. The reason is believed to be due to the acquisition system. As the top edges of the sandwich tube components touch the upper platen, which is connected to the load cell, the acquisition system only records a single data value. In other words, the data recorded by the load cell is an integral one which transfer to the load cell from the sandwich tube to the load cell as whole. In contrast, the data that is recorded during FE modeling or MLP algorithm is resulted from the multiple contacts between the sandwich tube components and the upper platen. Thus, there are many fluctuations in the force-displacement curves corresponding to the FEA and MLP results. For see the differences in the SEA, PCF values for the three methods they are compared in Figure 19b. The comparison shows that the error between the experimental values and the predicted values (i.e. the numerical and MLP results) is very small. The error in the PCF values between the experimental and

numerical simulation value and experimental and neural network prediction value is 0.1% and 0.1%, respectively. The error in the SAE values between the experimental and numerical simulation value and experimental and neural network prediction value is equal to 5.5% and 2.3%, respectively. This shows the accuracy of the model and the utilized algorithms for the optimization process.

7. Conclusion

The aim of this research was to optimize the geometrical parameters (the tube thickness, tube height and number of core tubes) and predict the force-displacement curve of bio-inspired aluminum sandwich tubes under quasi-static compression loading. In order to optimize the geometrical parameters, the PCF and SEA values, corresponding to the sandwich tube, were considered as the goal parameters.

According to the results obtained from the simulation of specimens, in general, it can be concluded that in samples with the same thickness and the same number of cores, the effects of height on the PCF and SAE values are insignificant (except for samples with 2.5 mm thick components). It also can be concluded that increasing the thickness has great effects on decreasing the PCF and increasing the SEA values. On the other hand, increasing the number of cores for samples with the same thickness and height increases the PCF, while this change has not created a predictable trend in the SAE parameter.

After analyzing the results obtained from the numerical simulation, the extracted force-displacement curves and the value of PCF and SEA corresponding to the simulated specimens are defined as the input data for the MLP and Levenberg– Marquardt's training algorithms to predict the force-displacement curve of the sandwich tube as energy absorption. By using this algorithm, the values of PCF and SAE parameters are predicted for a wide range of thicknesses, heights and different number of core tubes. By examining the PCF and SAE results obtained from the MLP, it can be concluded that the trend of changes of SEA and PCF, obtained from MLP algorithm, is identical to the trend which was observed in simulated samples.

Subsequently, the Genetic algorithm was employed to optimize the geometrical parameters. In this research, the optimization objectives are defined in a way where the PCF value is minimized and the SEA value is maximized.

Based on the results, a sandwich tube with the four core tubes, a thickness of 1 mm and a height of 92 mm would give the best performance. Experimental and numerical results that were obtained for the optimized sandwich tube design showed progressive failure with folding and buckling occurring. The samples showed similar behavior in the outer tube where a regular and square shape was formed.

After determining the optimal specimen, its force-displacement curve was predicted using MLP. Finally, the optimized specimen was simulated and the force displacement results, corresponding to the three methods employed (experimental, numerical and MLP) were compared. The PCF and SEA values and the force displacement curves obtained from the three methods were very similar, apart from a bit of discrepancy in the force displacement curves between the numerical and MLP methods and the experimental method, after the initial peak load. The maximum error between methods for the PCF value was 0.1% and for SAE value was 5.5%.

Disclosure statement

No potential conflict of interest was reported by the authors.

ORCID

Shahram Hosseini 🆔 http://orcid.org/0000-0002-4531-501X

References

[1] C. Kılıçaslan, M. Güden, İ. K. Odacı, and A. Taşdemirci, Experimental and numerical studies on the quasi-static and dynamic crushing responses of multi-layer trapezoidal aluminum corrugated sandwiches, Thin. Walled Struct., vol. 78, pp. 70–78, 2014. DOI: 10.1016/j.tws.2014.01.017.

[2] A. Mamalis, D. Manolakos, G. Demosthenous, and W. Johnson, Axial plastic collapse of thin bi-material tubes as energy dissipating systems, Int. J. Impact Eng., vol. 11, no. 2, pp. 185–196, 1991. DOI: 10.1016/0734-743X(91)90005-Z.

[3] N. San Ha, and G. Lu, A review of recent research on bio-inspired structures and materials for energy absorption applications, Compos. Part B: Engin., vol. 181, pp. 107496, 2020. DOI: 10.1016/j.compositesb.2019.107496.

[4] Y. Yu, and T. Fu, Dynamic response of the hybrid honeycomb sandwich panel with zero Poisson's ratio under low-speed impact, Mech. Adv. Mater. Struct., pp. 1–15, 2023. DOI: 10.1080/15376494.2023.2242421.

[5] X. Lv, Z. Xiao, J. Fang, Q. Li, F. Lei, and G. Sun, On safety design of vehicle for protection of vulnerable road users: a review, Thin. Walled Struct., vol. 182, pp. 109990, 2023. DOI: 10.1016/j.tws.2022.109990.

[6] A. Niknejad, M.M. Abedi, G.H. Liaghat, and M.Z. Nejad, Prediction of the mean folding force during the axial compression in foam-filled grooved tubes by theoretical analysis, Mater. & Design., vol. 37, pp. 144–151, 2012. DOI: 10.1016/j.matdes.2011.12.032.

[7] Q. Gao, G. Yin, C.C. Wang, and W.-H. Liao, Crushing and theoretical analysis of multi-cell tube filled with auxetic structure under axial impact loading, Mech. Adv. Mater. Struct., vol. 30, pp. 1–13, 2022. DOI: 10.1080/15376494.2022.2111730.

[8] M.O. Doudaran, H. Ahmadi, and G. Liaghat, Crushing performance of auxetic tubes under quasi-static and impact loading, J Braz. Soc. Mech. Sci. Eng., vol. 44, no. 6, pp. 230, 2022. DOI: 10.1007/s40430-022-03539-2.

[9] A. Tarafdar, G. Liaghat, H. Ahmadi, O. Razmkhah, S.C. Charandabi, M.R. Faraz, and E. Pedram, Quasi-static and low-velocity impact behavior of the bio-inspired hybrid Al/GFRP sandwich tube with hierarchical core: experimental and numerical investigation, Compos. Struct., vol. 276, pp. 114567, 2021. DOI: 10.1016/j.compstruct.2021.114567.

[10] A. Tarafdar, O. Razmkhah, H. Ahmadi, G. Liaghat, S. Chitsaz Charandabi, and M. Rezaei Faraz, Effect of layering layout on the energy absorbance of bamboo-inspired tubular composites, J. Reinf. Plast. Compos., vol. 41, no. 15–16, pp. 602–623, 2022. DOI: 10.1177/07316844211063865.

[11] S.P. Santosa, T. Wierzbicki, A.G. Hanssen, and M. Langseth, Experimental and numerical studies of foam-filled sections, Int. J. Impact Eng., vol. 24, no. 5, pp. 509–534, 2000. DOI: 10.1016/S0734-743X(99)00036-6.

[12] M.M. Abedi, R.J. Nedoushan, M. Sheikhzadeh, and W.-R. Yu, The crashworthiness performance of thin-walled ultralight braided lattice composite columns: experimental and finite element study, Compos. Part B: Engin., vol. 202, pp. 108413, 2020. DOI: 10.1016/j.compositesb.2020.108413.

[13] Y. Chen, X. Deng, H. Huang, H. Ran, and C. Wang, Crashworthiness of bionic tree-shaped hexagonal hierarchical gradient structures under oblique crushing conditions, Mech. Adv. Mater. Struct., pp. 1–21, 2023. DOI: 10.1080/15376494.2023.2240328.

[14] W. Wang, W. Ye, K. Huang, L. Xie, Q. Peng, F. Zhao, and H. Li, Impact-resistance mechanism of gradient ceramic/high entropy alloy composite structure, Mech. Adv. Mater. Struct., pp. 1–13, 2023. DOI: 10.1080/15376494.2023.2239814.

[15] G. Sun, D. Chen, G. Zhu, and Q. Li, Lightweight hybrid materials and structures for energy absorption: a state-of-the-art review and outlook, Thin. Walled Struct., vol. 172, pp. 108760, 2022. DOI: 10.1016/j.tws.2021.108760.

[16] F. Xu, Enhancing material efficiency of energy absorbers through graded thickness structures, Thin. Walled Struct., vol. 97, pp. 250–265, 2015. DOI: 10.1016/j.tws.2015.09.020.

[17] S. Saleh Mousavi-Bafrouyi, R. Eslami-Farsani, and A. Geranmayeh, The temperature effects on the mechanical properties of pseudo-ductile thin-ply unidirectional carbon-basalt fibers/epoxy hybrid composites with different stacking sequences, Fibers Polym., vol. 22, no. 11, pp. 3162–3171, 2021. DOI: 10.1007/s12221-021-1052-4.

[18] Y. Xiang, T. Yu, and L. Yang, Comparative analysis of energy absorption capacity of polygonal tubes, multi-cell tubes and honeycombs by utilizing key performance indicators, Mater. Design., vol. 89, pp. 689–696, 2016. DOI: 10.1016/j.matdes.2015.10.004.

[19] R. Yao, T. Pang, B. Zhang, J. Fang, Q. Li, and G. Sun, On the crashworthiness of thin-walled multi-cell structures and materials: state of the art and prospects, Thin. Walled Struct., vol. 189, pp. 110734, 2023. DOI: 10.1016/j.tws.2023.110734.

[20] A.A. Nia, and J.H. Hamedani, Comparative analysis of energy absorption and deformations of thin walled tubes with various section geometries, Thin. Walled Struct., vol. 48, no. 12, pp. 946–954, 2010.

[21] F.L. Palombini, F.M. Nogueira, W. Kindlein, S. Paciornik, J.E. de Araujo Mariath, and B.F. de Oliveira, Biomimetic systems and design in the 3D characterization of the complex vascular system of bamboo node based on X-ray microtomography and finite element analysis, J. Mater. Res., vol. 35, no. 8, pp. 842–854, 2020. DOI: 10.1557/jmr.2019.117.

[22] M.R. Faraz, H. Ahmadi, G. Liaghat, S. Vahid, O. Razmkhah, and A. Tarafdar, Energy absorption assessment of bio-mimicked hybrid Al/PP sandwich tube: experimental and Numerical

Investigation, Thin. Walled Struct., vol. 181, pp. 110116, 2022. DOI: 10.1016/j.tws.2022.110116.

[23] S. Guillow, G. Lu, and R. Grzebieta, Quasi-static axial compression of thin-walled circular aluminium tubes, Int. J. Mech. Sci., vol. 43, no. 9, pp. 2103–2123, 2001. DOI: 10.1016/S0020-7403(01)00031-5.

[24] Y. Zhang, Q. Liu, Z. He, Z. Zong, and J. Fang, Dynamic impact response of aluminum honeycombs filled with Expanded Polypropylene foam, Compos. Part B: Engin., vol. 156, pp. 17–27, 2019. DOI: 10.1016/j.compositesb.2018.08.043.

[25] L. Ying, T. Gao, W. Hou, M. Dai, X. Han, and D. Jiang, On crashing behaviors of bio-inspired hybrid multi-cell Al/CFRP hierarchical tube under quasi-static loading: an experimental study, Compos. Struct., vol. 257, pp. 113103, 2021. DOI: 10.1016/j.compstruct.2020.113103.

[26] M.M. Abedi, R.J. Nedoushan, and W.-R. Yu, Enhanced compressive and energy absorption properties of braided lattice and polyurethane foam hybrid composites, Int. J. Mech. Sci., vol. 207, pp. 106627, 2021. DOI: 10.1016/j.ijmecsci.2021.106627.

[27] B. Yilmaz, Additive manufacturing and characterization of mathematically designed bone scaffolds based on triply periodic minimal surface lattices, Mech. Adv. Mater. Struct., pp. 1–11, 2023. DOI: 10.1080/15376494.2023.2177913.

[28] X.H. Ni, X.G. Zhang, D. Han, Y. Zhang, W. Jiang, X.C. Teng, J. Hao, and X. Ren, Aluminum foam-filled auxetic double tubular structures: design and characteristic study, Mech. Adv. Mater. Struct., pp. 1–12, 2023. DOI: 10.1080/15376494.2023.2175397.

[29] W. Liu, Z. Lin, J. He, N. Wang, and X. Deng, Crushing behavior and multi-objective optimization on the crashworthiness of sandwich structure with star-shaped tube in the center, Thin. Walled Struct., vol. 108, pp. 205–214, 2016. DOI: 10.1016/j.tws.2016.08.021.

[30] K. Vinayagar, and A.S. Kumar, Crashworthiness analysis of double section bi-tubular thin-walled structures, Thin. Walled Struct., vol. 112, pp. 184–193, 2017. DOI: 10.1016/j.tws.2016.12.008.

[31] M.B. Francisco, J.L.J. Pereira, G.A. Oliver, L.R. Roque da Silva, S.S. Cunha, Jr, and G.F. Gomes, A review on the energy absorption response and structural applications of auxetic structures, Mech. Adv. Mater. Struct., vol. 29, no. 27, pp. 5823–5842, 2022. DOI: 10.1080/15376494.2021.1966143.

[32] W. Jiang, Y. Ao, J. Liu, J. Liu, and W. Huang, Dynamic responses and failure mechanism of composite double-arrow auxetic structure under impact loading, Mech. Adv. Mater. Struct., vol. 30, no. 13, pp. 2593–2609, 2023. DOI: 10.1080/15376494.2022.2059600.

[33] M. Oloumi Doudaran, H. Ahmadi, G.H. Liaghat, and M. Seidi, Experimental and numerical investigation on crashworthiness of composite reinforced auxetic cellular tubes, Mech. Adv. Mater. Struct., pp. 1–23, 2023. DOI: 10.1080/15376494.2023.2248115.

[34] W. Ma, S. Xie, Z. Li, Z. Feng, and K. Jing, Crushing behaviors of horse-hoof-wall inspired corrugated tubes under multiple loading conditions, Mech. Adv. Mater. Struct., vol. 29, no. 22, pp. 3263–3280, 2022. DOI: 10.1080/15376494.2021.1892245.

[35] Y. Xiao, H. Yin, H. Fang, and G. Wen, Crashworthiness design of horsetail-bionic thin-walled structures under axial dynamic loading, Int J Mech Mater Des., vol. 12, no. 4, pp. 563–576, 2016. DOI: 10.1007/s10999-016-9341-6.

[36] B. Chen, M. Zou, G. Liu, J. Song, and H. Wang, Experimental study on energy absorption of bionic tubes inspired by bamboo structures under axial crushing, Int. J. Impact Eng., vol. 115, pp. 48–57, 2018. DOI: 10.1016/j.ijimpeng.2018.01.005.

[37] M.H. Al Shamisi, A.H. Assi, and H.A. Hejase, Using MATLAB to develop artificial neural network models for predicting global solar radiation in Al Ain City–UAE. In Engineering education and research using MATLAB, Citeseer, 2011.

[38] G.X. Gu, C.-T. Chen, D.J. Richmond, and M.J. Buehler, Bioinspired hierarchical composite design using machine learning: simulation, additive manufacturing, and experiment, Mater.

Horiz., vol. 5, no. 5, pp. 939–945, 2018. DOI: 10.1039/C8MH00653A.

[39] P. Malik, A. Gehlot, R. Singh, L.R. Gupta, and A.K. Thakur, A review on ANN based model for solar radiation and wind speed prediction with real-time data, Arch Computat Methods Eng., vol. 29, no. 5, pp. 3183–3201, 2022. DOI: 10.1007/s11831-021-09687-3.

[40] Z. Li, W. Ma, S. Yao, P. Xu, L. Hou, and G. Deng, A machine learning based optimization method towards removing undesired deformation of energy-absorbing structures, Struct Multidisc Optim., vol. 64, no. 2, pp. 919–934, 2021. DOI: 10.1007/s00158-021-02896-1.

[41] S.S. Subbiah, and J. Chinnappan, A Review of Bio-Inspired Computational Intelligence Algorithms in Electricity Load Forecasting, Smart Buildings Digitalization, vol. 24, pp. 169–192, 2022.

[42] A. Faramarzi, N. Loghmani, R. Moghadam, A. Allahverdy, and M.S. Mansoory, Semi-automated glioblastoma tumor detection based on different classifiers using magnetic resonance spectroscopy, FBT., vol. 8, 2021. DOI: 10.18502/fbt.v8i3.7113.

[43] Y. Amellas, A. Djebli, A. Echchelh, and R. Jestr, Levenberg-Marquardt training function using on MLP, RNN and Elman neural network to optimize hourly forecasting in Tetouan City (Northern Morocco), JESTR., vol. 13, no. 1, pp. 67–71, 2020. DOI: 10.25103/jestr.131.09.

[44] K. Liu, Q. Liu, M.A. El-Meligy, and M. Sharaf, Application of artificial intelligence and numerical method to improve the natural oscillation of the sport mountain bike tires, Mech. Adv. Mater. Struct., pp. 1–21, 2023. DOI: 10.1080/15376494.2023.2235339.

[45] A. Sadrmomtazi, J. Sobhani, and M. Mirgozar, Modeling compressive strength of EPS lightweight concrete using regression, neural network and ANFIS, Constr. Build. Mater., vol. 42, pp. 205–216, 2013. DOI: 10.1016/j.conbuildmat.2013.01.016.

[46] R. Kalantari, R. Moqadam, N. Loghmani, A. Allahverdy, M.B. Shiran, and A. Zare-Sadeghi, Brain tumor segmentation using hierarchical combination of fuzzy logic and cellular automata, J. Med. Signals Sens., vol. 12, no. 3, pp. 263–268, 2022. DOI: 10.4103/jmss.jmss_128_21.

[47] R. Moqadam, N. Loghmani, M.S. Mansoori, and A. Allahverdy, Combination of classifiers to detect grade of glioblastoma using MRS, 2022 30th International Conference on Electrical Engineering (ICEE), IEEE; pp. 8–11, 2022. DOI: 10.1109/ICEE55646.2022.9827010.

[48] M. Shakir, M. Talha, and A.D. Dileep, Machine learning based probabilistic model for free vibration analysis of functionally graded graphene nanoplatelets reinforced porous plates, Mech. Adv. Mater. Struct., pp. 1–14, 2023. DOI: 10.1080/15376494.2023.2225051.

[49] M. Moshtaghzadeh, A. Bakhtiari, E. Izadpanahi, and P. Mardanpour, Artificial Neural Network for the prediction of fatigue life of a flexible foldable origami antenna with Kresling pattern, Thin. Walled Struct., vol. 174, pp. 109160, 2022. DOI: 10.1016/j.tws.2022.109160.

[50] M. Berradia, E.H. Meziane, A. Raza, M. Ahmed, QuZ Khan, and F. Shabbir, Prediction of ultimate strain and strength of CFRP-wrapped normal and high-strength concrete compressive members using ANN approach, Mech. Adv. Mater. Struct., pp. 1–23, 2023. DOI: 10.1080/15376494.2023.2219441.

[51] Z. Li, W. Ma, H. Zhu, G. Deng, L. Hou, P. Xu, and S. Yao, Energy absorption prediction and optimization of corrugation-reinforced multicell square tubes based on machine learning, Mech. Adv. Mater. Struct., vol. 29, no. 26, pp. 5511–5529, 2022. DOI: 10.1080/15376494.2021.1958032.

[52] W. Yang, G. Yan, E.M. Awwad, and M. Al-Razgan, AI-based solution on the efficient structural design of the graphene-platelets reinforced concrete ceilings, Mech. Adv. Mater. Struct., pp. 1–24, 2023. DOI: 10.1080/15376494.2023.2217653.

[53] M.A. Bessa, P. Glowacki, and M. Houlder, Bayesian machine learning in metamaterial design: fragile becomes

supercompressible, Adv. Mater., vol. 31, no. 48, pp. 1904845, 2019. DOI: 10.1002/adma.201904845.

[54] S. Gowid, E. Mahdi, and F. Alabtah, Modeling and optimization of the crushing behavior and energy absorption of plain weave composite hexagonal quadruple ring systems using artificial neural network, Compos. Struct., vol. 229, pp. 111473, 2019. DOI: 10.1016/j.compstruct.2019.111473.

[55] A. Hojjati, M. Monadi, A. Faridhosseini, and M. Mohammadi, Application and comparison of NSGA-II and MOPSO in multi-objective optimization of water resources systems, J. Hydrol. Hydromech., vol. 66, no. 3, pp. 323–329, 2018. DOI: 10.2478/johh-2018-0006.

[56] H. Monsef, M. Naghashzadegan, A. Jamali, and R. Farmani, Comparison of evolutionary multi objective optimization algorithms in optimum design of water distribution network, Ain Shams Eng. J., vol. 10, no. 1, pp. 103–111, 2019. DOI: 10.1016/j.asej.2018.04.003.

[57] D. Chicco, M. J. Warrens, and G. Jurman, The coefficient of determination R-squared is more informative than SMAPE, MAE, MAPE, MSE and RMSE in regression analysis evaluation, PeerJ Comput. Sci., vol. 7, pp. e623, 2021. DOI: 10.7717/peerj-cs.623.